Analysis of the Suspended Strip in Elliptical Cross Section by Separation of Variables

Tullio Rozzi, *Fellow, IEEE,* Luca Pierantoni, *Member IEEE,* and Marco Ronzitti

***Abstract*— The coaxial suspended strip configuration in elliptical cross section is often found in transitions from ordinary coax to planar circuits and other geometries. Using elliptical coordinates makes the problem separable, leading to closed-form solutions for the fundamental TEM mode and the TE/TM higher modes. It is emphasized that the presence of the thin strip is dealt with analytically by this approach. Mode patterns and TEM characteristic impedance are reported. The cutoff frequencies versus eccentricity are computed for the first eight modes.**

***Index Terms*— Elliptical coordinates, strips.**

I. Introduction

A THIN metallic strip centrally suspended in a hollow conductor of elliptical cross section, as shown in Fig. 1, constitutes a coaxial-like TEM transmission line, where TEM characteristic impedance and mode pattern can be controlled by varying the strip width and eccentricity.

Apart from its own merit, it can be found in transitions from ordinary coax to coplanar waveguide (CPW) and other planar guides or from coax to TEM cells [1].

Although the fundamental TEM mode of the cross section of Fig. 1 can be analyzed by conformal mapping [2], [3], its higher order TE/TM modes involve solution of the wave equation with boundary conditions on the elliptic conductor and in presence of sharp-edge conditions at the strip extremities. The latter problem can also be solved by a variety of methods, such as variational techniques, transverse resonance, or numerical methods such as finite elements of finite-difference time domain (FDTD). This configuration, however, also provides an instructive test-bed for a direct solution of the wave equation by the method of separation of coordinates, once the appropriate system of coordinates is selected. The latter is seen to be the elliptic cylinder system, where the inner strip conductor is the limiting case of an ellipse of unit eccentricity.

Separation of "radial" and "angular" dependencies leads to the well-known Mathieu's equation, the solutions of which are fairly well documented [4], [5] and currently available in standard mathematical codes [6].

The closed-form analysis very simply produces the fundamental TEM mode (see Fig. 2) while also highlighting the existence of two types of higher modes, first reported in [7] in connection with ridged waveguides. The first kind is found in closed elliptical waveguides and is perfectly "regular," that is, it neither feels the presence of the strip nor presents edge singularities. The latter kind, however, being closely linked to the presence of the strip, displays the typical singular square root behavior.

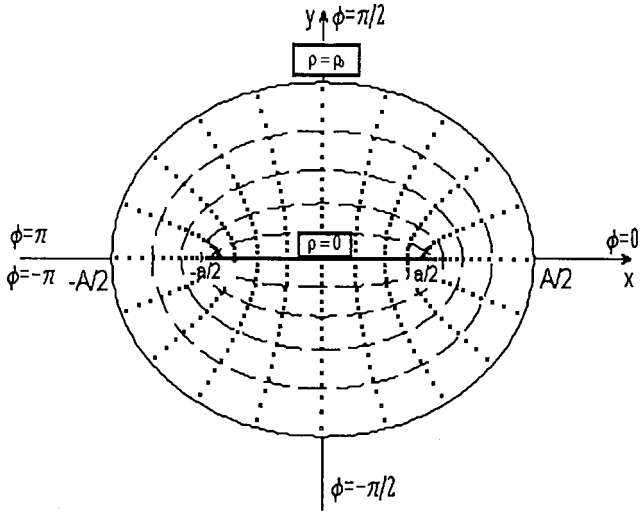

Fig. 1. Cross-section geometry and coordinate system.

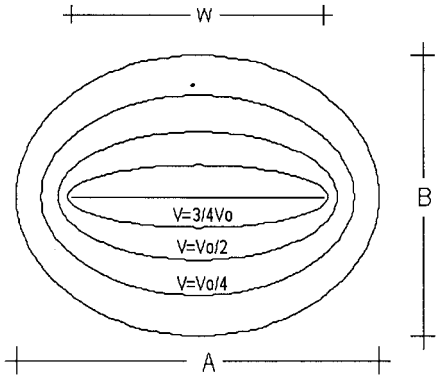

Fig. 2. Equipotential curves on the cross section. (These curves were plotted for a value of eccentricity equal to 0.7).

Characteristic impedance and mode pattern of the fundamental mode are reported versus the eccentricity, whereas cutoff frequencies and mode patterns are computed for the first eight TE and TM modes of both kinds above.

II. Theory

A. Cross-Section Geometry

Let us consider the structure shown in Fig. 1 which is cylindrical and uniform along the **z**-direction of propagation. It

Manuscript received February 26, 1996; revised October 18, 1996.

T. Rozzi is with the Department of Electronics and Control, University of Ancona, 60131 Ancona, Italy.

L. Pierantoni and M. Ronzitti are with the Department of Electronics and Automatics, University of Ancona, 60131 Ancona, Italy.

Publisher Item Identifier S 0018-9480(97)00832-6.

consists of an outer conductor of elliptical form, and an inner strip conductor extending between the two focal points of the ellipse; both conductors are ideal. This cross section can be described in terms of an elliptical cylindrical coordinate system $(\rho,\ \phi,\ \mathbf{z})$ that is connected to the Cartesian one $(\mathbf{x},\ \mathbf{y},\ \mathbf{z})$ by means of the following relationships [4], [7]:

$$x = \frac{a}{2}\cosh(\rho)\cos(\phi)$$
$$y = \frac{a}{2}\sinh(\rho)\sin(\phi). \tag{1a}$$

The elliptical outer boundary of the guide is described by the locus:

$$\rho = \rho_0, \qquad -\pi < \phi < \pi \tag{1b}$$

whereas the inner strip of width a, can be seen as a degenerate ellipse given by

$$\rho = 0, \qquad -\pi < \phi < \pi. \tag{1c}$$

The geometrical characteristics of the section can be usefully summarized by a single parameter, its eccentricity e, defined as follows:

$$e = \frac{a}{A} \tag{1d}$$

where $\mathbf{A}$ is the major axis of the elliptical outer conductor that is expressible in terms of a, ρ_0 as

$$A = a\cosh(\rho_0). \tag{1e}$$

B. Solution of the Wave Equation

The electromagnetic wave propagation in the above cylindrical guide can be described in terms of a scalar-wave function Ψ satisfying the Helmholtz equation:

$$\nabla^2\Psi + k_c^2\Psi = 0 \tag{2}$$

with

$$k_c^2 = k^2 - \beta^2 \tag{2a}$$

being k_c the transverse component of the wavenumber $\mathbf{k} = \omega/\mathbf{c}$.

In terms of elliptical coordinates, the Helmholtz equation can be rewritten as follows:

$$\left[\frac{\partial^2}{\partial\rho^2} + \frac{\partial^2}{\partial\phi^2} + \left(\frac{a\cdot k_c}{2}\right)\left(\cosh^2\rho - \cos^2\phi\right)\right]\cdot\Psi = 0. \tag{3}$$

Equation (3) separates in elliptic cylinder coordinates. As a consequence, the scalar-wave function Ψ can be represented as the product:

$$\Psi = \Phi(\phi)\cdot R(\rho). \tag{4}$$

The wave function Ψ must also be continuous with continuous first derivatives at all points of the region except, at most, isolated points on the boundary where it may have quadratically integrable singularities.

The azimuthal function Φ and the radial function $\mathbf{R}$ may be determined from the two differential equations:

$$\Phi'' + (b^2 - h^2\cos^2\phi)\cdot\Phi = 0 \tag{5a}$$

$$-R'' + (b^2 - h^2\cosh^2\rho)\cdot R = 0 \tag{5b}$$

where b is the separation constant and h is defined as

$$h = \frac{a\cdot k}{2}. \tag{5c}$$

Equation (5a) is the Mathieu's equation, while (5b) is the modified Mathieu's equation. The proper azimuthal solutions are those having periods of π and 2π, and, therefore, Φ is the Mathieu function of either odd or even types denoted by $S_{o_n}(h,\phi)$ and $S_{e_n}(h,\phi)$, respectively. The value of the separation constant is completely defined by this choice and $\mathbf{b}$ takes the values b_{o_n} and b_{e_n}, where these quantities are the eigenvalues corresponding to odd or even periodic Mathieu functions. Two types of radial functions correspond to each value of h and b. They may be denoted by $J_{o_n}(h,\rho)$ and $N_{o_n}(h,\rho)$, or $J_{e_n}(h,\rho)$ and $N_{e_n}(h,\rho)$, and they correspond to Bessel and Neumann functions in circular cylindrical coordinates. For details and properties of these functions, the reader is referred to [4] and [5].

III. Fundamental TEM-Mode Analysis

In order to obtain the TEM mode we set $k_c = 0$; then $k = \beta$ and the wave equation (2) reduces to the Laplace's equation for the quasistatic potential:

$$\nabla^2\Psi = 0. \tag{6}$$

If the inner-strip potential is set equal to $\mathbf{V}_o$, the solution of (6) is simply given by

$$\Psi = V_o\left(1 - \frac{\rho}{\rho_o}\right). \tag{7}$$

The electric and magnetic fields are derived by means of the following relationships:

$$\mathbf{E} = -\nabla\Psi \tag{8}$$

hence,

$$\mathbf{E} = E_\rho\cdot\hat{\rho} = \frac{V_o}{g\cdot\rho_o} \tag{8a}$$

$$\mathbf{H} = H_\phi\cdot\hat{\phi} = \frac{1}{\eta}E_\rho\cdot\hat{\phi} \tag{8b}$$

being

$$g = \frac{a}{2}\sqrt{\sinh^2\rho + \sin^2\phi} \tag{8c}$$

a "metric" scale factor, and

$$\eta = \sqrt{\frac{\mu_o}{\epsilon_o}} \tag{8d}$$

the free-space wave impedance.

IV. Characteristic TEM Impedance

The characteristic TEM impedance is obtained from the computation of the distributed capacitance and inductance of the line-per-unit length.

A. Capacitance-per-unit Length

Referring to Fig. 1, after setting $\theta = \cos^{-1}(2x/a)$, where x is the abscissa on the strip (i.e., for $y = 0$), the charge density σ is given by

$$\sigma = \frac{2\varphi(V/\rho_o)}{a|\sin\theta|} \tag{9}$$

and the total charge per unit length on the strip is

$$Q = \frac{a}{2}\int_0^{2\pi} \sigma|\sin\theta|d\theta = 2\pi\epsilon\frac{V}{\rho_o} \tag{10}$$

hence, the capacitance-per-unit length:

$$C = \frac{Q}{V} = \frac{2\pi\epsilon}{\rho_o} \tag{11}$$

is plotted in Fig. 4 versus the eccentricity e.

B. Inductance-per-unit Length

Ampere's law gives the current on the strip as

$$I = \oint \mathbf{H}\cdot\mathbf{dl} = \frac{V_o}{\eta\rho_o}\int_{-\pi}^{\pi}\frac{1}{g}\cdot g d\phi = \frac{2V_o\pi}{\eta\rho_o}. \tag{12}$$

Although the integration path is arbitrary, choosing an ellipse that is confocal with the outer conductor simplifies the evaluation. Furthermore, we have

$$L\cdot I = \int_S \mathbf{B}\cdot\mathbf{dS}. \tag{13}$$

The result of combining (12) and (13) is

$$L = \frac{\mu_o}{2\pi}\rho_o. \tag{14}$$

C. Characteristic Impedance

The characteristic TEM impedance is defined as follows:

$$Z_o = \sqrt{\frac{L}{C}} = \eta\frac{\rho_o}{2\pi} \tag{15}$$

and is plotted in Fig. 4 versus the eccentricity e.

By inspection we can see that

$$\sqrt{LC} = \frac{\mu_o}{2\pi}\rho_o\cdot\frac{2\pi\epsilon}{\rho_o} = \sqrt{\mu_o\epsilon} = \frac{1}{c}. \tag{16}$$

Looking at the plot of the characteristic impedance Z_o versus the eccentricity e, we note that as $e \approx 0.8$, $Z_0 \approx 50\ \Omega$, as suitable for applications.

V. Higher Order Modes Analysis

The solutions of the Helmholtz's equation can be separated in the following two sets of modes, each having even/odd symmetry with respect to the $\mathbf{y} = 0$ axis: 1) TE modes, for which it is $\Psi = H_z$, and 2) TM modes, for which we have $\Psi = E_z$.

We now consider their propagation behavior in detail.

A. TE Modes

Apart from the particular type of symmetry considered, these types of modes must satisfy the boundary condition of the maximum tangential magnetic field on the conductor:

$$\frac{\partial\Psi}{\partial\rho}|_{\rho=\rho_0} = 0 \text{ and } \frac{\partial\Psi}{\partial\rho}|_{\rho=0} = 0, \qquad \text{for } -\pi \le \phi \le \pi. \tag{17a}$$

1) TE Even Modes: In order for H_z to be even with respect to the $y = 0$ axis, we require

$$\frac{\partial\psi}{\partial\phi} = 0, \qquad \text{for } \phi = -\pi,\ \pi,\ 0. \tag{17b}$$

Hence, the wave function $\Psi = H_z$ will assume the form:

$$Hz = S_{e_n}(h,\ \phi)\cdot J_{e_n}(h,\ \rho), \qquad n = 0,\ 1,\ 2. \tag{18}$$

These types of modes are characterized by the absence of the electric field component along the x-axis; as a consequence, they may also exist in elliptical hollow guides without the loading strip and they are well known in the literature [9]. We denote these modes by the symbol $\mathbf{TE^e_{nm}}$.

The eigenvalues are computed by imposing the boundary condition on the guide walls, yielding the dispersion equation:

$$\frac{\partial}{\partial\rho}J_{e_n}(h_c,\ \rho_o) = 0 \quad \text{with } k_c = \frac{2h_c}{a}. \tag{19}$$

2) TE Odd Modes: For these modes (17a) still holds, but we require H_z to be odd at $y = 0$ outside the strip, that is

$$Hz = 0, \qquad \text{for } \phi = -\pi,\ \pi,\ 0. \tag{20}$$

A wave function $\Psi = H_z$ satisfying (17a) and (20) can be selected as follows:

$$Hz = S_{o_n}(h,\ \phi)\cdot R_{o_n}(h,\ \rho), \qquad n = 1,\ 2,\ 3,\cdots \tag{21a}$$

with

$$R_{o_n}(h,\ \rho) = J_{o_n}(h,\ \rho) - \frac{J'_{o_n}(h,\ 0)}{N'_{o_n}(h,\ 0)}\cdot N_{o_n}(h,\ \rho). \tag{21b}$$

Equation (21b) is chosen with a view to satisfying the boundary conditions on the strip (i.e., $R'_{o_n}(h,\ 0) = 0$). These modes are denoted by $\mathbf{TE^s_{nm}}$.

By enforcing the boundary condition on the guide walls, we derive the corresponding dispersion equation:

$$\frac{\partial}{\partial\rho}R_{o_n}(h_c,\ \rho_o) = 0. \tag{22}$$

It is noted that the fields are now singular at the strip edges, and these modes can only exist in the strip-loaded guide.

B. TM Modes

Vanishing of $\Psi = E_z$ on the conductors implies:

$$\Psi(\rho,\ \phi) = 0, \qquad \text{for } \rho = \rho_o,\ 0. \tag{23}$$

1) TM Even Modes: In this case we set Ψ equal to E_z, so that Ψ must vanish on the strip while at its sides we have

$$\left.\frac{\partial \Psi}{\partial \phi}\right|_{\phi=\pm\pi,\,0} = 0. \tag{24}$$

Hence, we have to select $\Psi = E_z$ as

$$Ez = S_{e_n}(h,\,\phi)\cdot R_{e_n}(h,\,\rho), \qquad n = 0,\,1,\,2,\,3,\cdots \tag{25a}$$

where

$$R_{e_n}(h,\,\rho) = J_{e_n}(h,\,\rho) - \frac{J_{e_n}(h,\,0)}{N_{e_n}(h,\,0)}\cdot N_{e_n}(h,\,\rho). \tag{25b}$$

Equation (25b) is chosen so as to satisfy the boundary condition on the strip (i.e., $R_{e_n}(h,\,0) = 0$). From (24) and (25), it follows that such modes may only exist in the presence of the strip. They are denoted by $\mathbf{TM^s_{nm}}$ and their cutoff wavenumbers are obtained from

$$R_{e_n}(h_c,\,\rho_o) = 0. \tag{26}$$

2) TM Odd Modes: They may exist even in the absence of the strip (elliptical waveguide) [9]; in this case, the wave function $\Psi = E_z$ becomes odd with respect to the x-axis, due to symmetry. Moreover, the x-component of the electric field vanish on the strip as given in (23), as well as at its sides, that is,

$$\Psi(\rho,\,\phi) = 0, \qquad \text{for } \phi = -\pi,\,\pi,\,0. \tag{27}$$

Hence,

$$E_z = S_{o_n}(h,\,\phi)\cdot J_{o_n}(h,\,\rho), \qquad n = 0,\,1,\,2,\cdots. \tag{28}$$

These modes are denoted with $\mathbf{TM^e_{nm}}$ and their cutoff wavenumbers are obtained from

$$J_{o_n}(h_c,\,\rho_o) = 0. \tag{29}$$

In the Appendix we report the expressions of the TE/TM fields.

VI. Method

In comparison with the analytical solution, we also have computed TEM characteristic impedance and cutoff wavelengths of the TE/TM higher order modes, utilizing the finite-element method (FEM) method. Since this method is well known [8], we only report an important particular involved in its implementation—the choice of the discretizing grid. Referring to Fig. 3, we note that the grid topology is chosen in order to fit the coordinate system. Taking into account that the cross section is symmetric along the x and y axes, we only consider one quadrant.

We divide the geometrical area in n_ρ ellipses, each corresponding to a particular value ρ of the radial coordinates:

$$\rho = i\cdot\frac{\rho_0}{n_p}, \qquad i = 0,\,1,\,2,\cdots,n_\rho$$

and in n_ϕ hyperbolas, each corresponding to a value ϕ of the angular coordinate:

$$\phi = \frac{\pi}{2} - j\cdot\frac{\pi}{2\cdot n_\phi}, \qquad j = 0,\,1,\,2,\cdots,n_\phi.$$

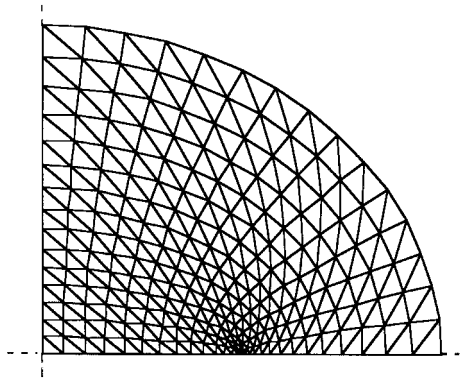

Fig. 3. The grid used for the computation with the FEM method.

Thus, using triangular elements, their number is

$$N = 2^*(n\rho+1)^*(n_\phi+1).$$

1) TEM Characteristic Impedance: In order to find the TEM characteristic impedance we must first determine the distribution of the potential on the cross section (the solution of Laplace's equation). By imposing the boundary conditions on the inner strip and on the outer conductor ($V = 1$ on the former and $V = 0$ on the latter). Once the potential is known at all grid points, we compute the total charge on the strip using Gauss' law:

$$Q = \oint D\cdot dl = \epsilon\oint\frac{\partial V}{\partial n}\,dl.$$

If we number the nodes (i.e., the grid points) in the clockwise direction, starting from the lower left corner of Fig. 3, the nodes on the **i**th ellipse will be numbered as

$$(i-1)^*(n_\phi+1)+j+1$$

where

$$i = 1,\,2,\cdots,(n_\rho+1) \text{ and } j = 1,\,2,\cdots,(n_\phi+1).$$

By choosing one of these ellipses, for example the i_oth, as an integration path, Gauss' law becomes

$$Q = 4\sum_{j=1}^{n_\phi}\left[V_{(i_o-1)\cdot(n_\phi+1)+j+1} - V_{i_o\cdot(n_\phi+1)+j+1}\right]\cdot\frac{\Delta\phi}{\Delta\rho}$$

with

$$\Delta\phi = \frac{\pi}{2\cdot n_\phi} \text{ and } \Delta\rho = \frac{\rho_0}{n_\rho}.$$

The factor 4 is due to the fact that we are considering only one-quarter of the cross section. We note that the j-index of the summation must be stopped at n_ϕ, in order to not compute the nodes on the x-axis twice.

The capacitance-per-unit length is now found as:

$$C = \frac{Q}{V_o} = Q$$

where we set $V_o = 1$.

Finally, the TEM characteristic impedance is computed as

$$Z_o = \frac{1}{c\cdot C}$$

where c is the phase velocity of light in the free space.

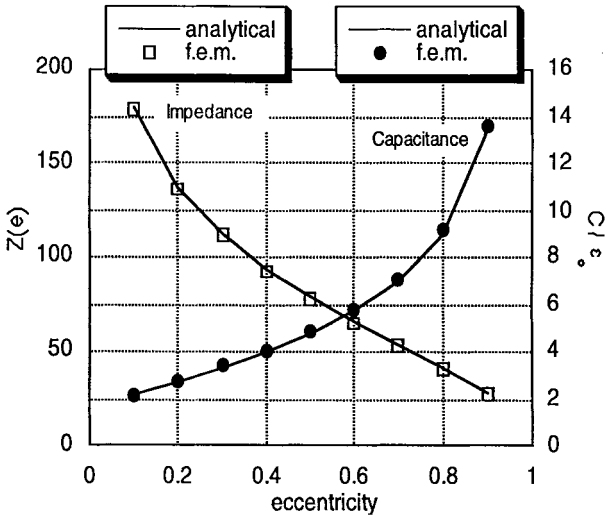

Fig. 4. Comparison between analytical and numerical (**FEM**) data of the characteristic TEM impedance and of the normalized capacitance (ratio $C/\epsilon o$) per-unit length, plotted versus the eccentricity of the cross section.

TABLE I
COMPARISON BETWEEN ANALYTICAL AND CORRESPONDING FEM VALUES OF THE NORMALIZED CAPACITANCE-PER-UNIT LENGTH AND OF THE CHARACTERISTIC IMPEDANCE FOR DIFFERENT VALUES OF THE ECCENTRICITY OF THE CROSS SECTION

e	0.1	0.2	0.3	0.4	0.5	0.6	0.7	0.8	0.9
C/ϵ_0									
F.E.M.	2.1092	2.7574	3.3777	4.0444	4.8189	5.7825	7.1011	9.1900	13.607
analytical	2.0991	2.7408	3.3531	4.0102	4.7710	5.7192	7.0157	9.0647	13.450
error(%)	0.48	0.60	0.73	0.85	1.00	1.10	1.21	1.38	1.17
Z_0									
F.E.M.	178.49	136.53	111.46	93.09	78.13	65.11	53.02	40.97	27.67
analytical	179.59	137.55	112.43	94.01	79.02	65.92	53.74	41.59	28.03
error(%)	0.61	0.73	0.86	0.98	1.12	1.23	1.33	1.49	1.29

2) TE/TM Higher Order Modes: As can be found in [8], the procedure is well known and only a brief mention is given. Considering for TE modes the Hz-component and for TM modes the Ez-component, we computed the stationary points of the following functional:

$$I(\Phi) = \frac{1}{2}\int\int [|\nabla^2\Phi| - k^2\Phi] \cdot dS$$

where Φ can be either Hz or Ez.

This, in turn, leads to the problem of finding eigenvalues and eigenvectors of a sparse matrix, where the eigenvalues represent the squares of the transverse constant of propagation and the eigenvectors the values of Hz/Ez at all the grid points. By inspection of these latter quantities we recognize the kind of mode (i.e., the index m, n in the form $\mathbf{TE_{m,n}}$ and $\mathbf{TM_{m,n}}$) corresponding to each eigenvalue.

VII. NUMERICAL RESULTS

In Fig. 4 we compare the analytical results with the numerical ones obtained by the FEM method. We report TEM characteristic impedance and normalized capacitance versus eccentricity; the two sets of data are in excellent agreement as can be verified from the relative percentages of errors reported in Table I.

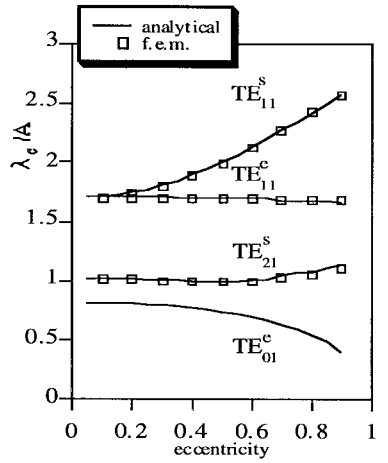

(a)

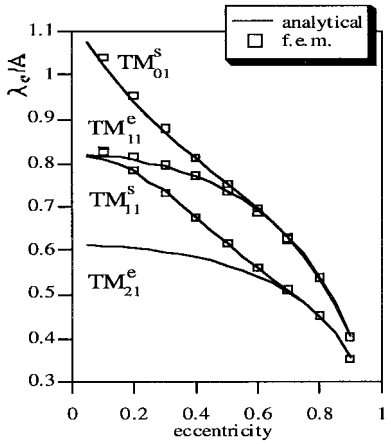

(b)

Fig. 5 Comparison between analytical and numerical (**FEM**) data of the normalized cutoff wavelengths versus the eccentricity of the cross section, for the first higher order TE modes. (a) First mode comparison. (b) Second mode comparison.

In Fig. 5(a) and (b) we report the cutoff frequencies for the first two modes of each of the four types of Section V, evaluated both analytically and by means of the FEM program. The normalized wavelengths are plotted versus the eccentricity of the cross section; the normalization constant is the major axis of the ellipse. In Table II, (a) and (b) are reported the numerical values of these quantities; as can be seen, the agreement between analytical and FEM data seems to be very good over a wide range of eccentricities. The less accurate results are obtained in correspondence of the values at the edges of the range; in fact, for eccentricity too near to zero or to unity, the FEM method suffers from the divergence of the fields, while the analytical model gives exact results.

The Mathieu radial functions involved in the above calculations were computed by utilizing their Bessel expansions [4]–[6].

We may note, as in [7], that for values of eccentricity less than 0.3 the ratio

$$\frac{B}{A} = \tanh \rho_o \tag{30}$$

TABLE II
COMPARISON BETWEEN ANALYTICAL AND FEM DATA OF THE NORMALIZED CUTOFF WAVELENGTHS WITH THE RELATIVE PERCENTAGE OF ERROR. (a) FOR THE FIRST HIGHER-ORDER TE MODES. (b) FOR THE FIRST HIGHER-ORDER TM MODES

e	0.1	0.2	0.3	0.4	0.5	0.6	0.7	0.8	0.9
TE^e_{11}									
F.E.M	1.690	1.694	1.695	1.695	1.693	1.690	1.686	1.681	1.674
analytical	1.706	1.705	1.702	1.699	1.693	1.692	1.684	1.680	1.669
error(%)	0.92	0.63	0.43	0.23	0.01	0.08	0.15	0.05	0.31
TE^s_{11}									
F.E.M.	1.699	1.735	1.801	1.885	1.997	2.127	2.268	2.416	2.564
analytical	1.715	1.749	1.809	1.896	2.007	2.135	2.273	2.418	2.565
error(%)	0.98	0.83	0.44	0.61	0.49	0.36	0.22	0.09	0.02
TE^s_{21}									
F.E.M.	1.011	1.007	0.999	0.992	0.989	0.997	1.020	1.056	1.099
analytical	1.025	1.019	1.009	1.001	0.998	1.009	1.037	1.077	1.124
error(%)	1	1	1	1	1	1	2	2	2

(a)

e	0.1	0.2	0.3	0.4	0.5	0.6	0.7	0.8	0.9
TM^e_{01}									
F.E.M.	1.042	0.952	0.877	0.812	0.753	0.695	0.628	0.539	0.404
analytical	1.02	0.94	0.87	0.81	0.75	0.70	0.63	0.54	0.40
error(%)	2.16	1.29	0.86	0.23	0.37	0.77	0.35	0.17	1.00
TM^e_{11}									
F.E.M.	0.829	0.815	0.797	0.771	0.736	0.689	0.627	0.539	0.404
analytical	0.82	0.81	0.79	0.77	0.74	0.69	0.63	0.54	0.41
error(%)	1.06	0.65	0.84	0.09	0.55	0.09	0.52	0.19	1.46
TM^s_{11}									
F.E.M.	0.823	0.784	0.733	0.675	0.615	0.560	0.509	0.449	0.353
analytical	0.81	0.78	0.74	0.68	0.62	0.56	0.51	0.45	0.35
error(%)	1.65	0.54	0.92	0.74	0.76	0.00	0.22	0.24	0.74

(b)

is very close to unity, hence, when the cross section is nearly circular, the hollow-guide modes ($\mathbf{TE^e_{nm}}$ and $\mathbf{TM^e_{nm}}$) tend to the correspondent ones of the circular waveguide.

In Fig. 6(a) and (b), we compare the radial and the angular component of the electric field for the first TE higher mode, obtained by the present analytical method, with the corresponding ones evaluated by means of the FEM method. We observe a generally good agreement, apart from the field near the strip edges, where the FEM results are less accurate because of the inevitable discretizing error involved in the numerical method itself.

In the computation with the FEM method we note that a 450-element grid gives an error which is less than 2/3%. The grid topology (see Fig. 3) is the same as the coordinate system with 15 divisions for both the radial coordinate and the azimutal coordinate (using triangular elements this gives: $2^*(15^*15) = 450$ elements). The computation time in this case was about 15 min for each value of eccentrity, against 5 min needed for the analytical computation (not optimized). The PC used for this computation is equipped with an 486-100 MHz processor and 12-Mb RAM; all the programs were implemented in MATLAB.

VIII. CONCLUSION

The suspended strip in elliptical cross section is solved analytically in elliptical coordinates, obtaining field patterns and characteristic impedance versus eccentricity of the fundamental TEM mode in closed form.

Higher order TE and TM modes of two kinds are also found analytically: 1) those that would also exist in an empty elliptical guide; and 2) those solely due to the presence of the strip conductor featuring singular behavior at the strip edges.

Cutoff frequencies and mode patterns of the lowest eight modes are in excellent agreement with the results of the FEM analysis.

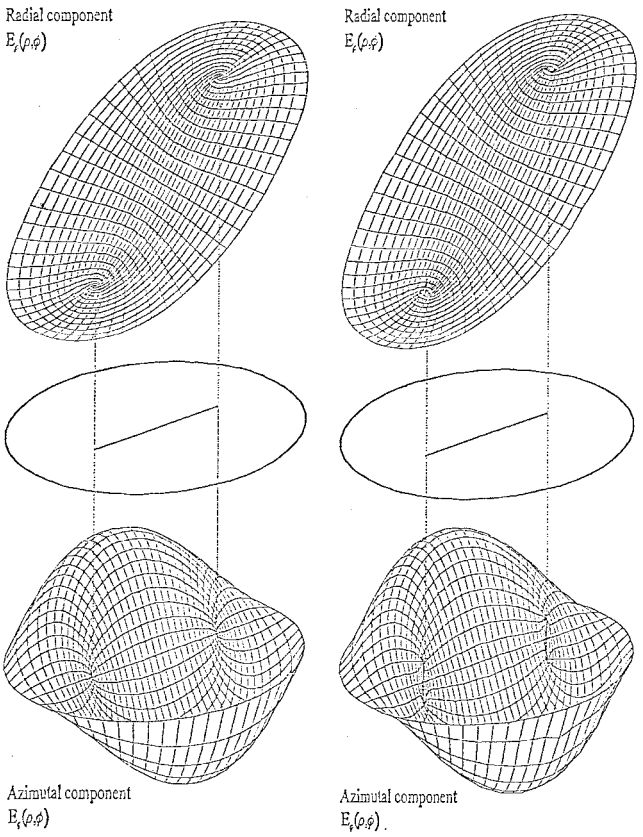

Fig. 6. Comparison of the electric field component for the first higher order TE mode. (a) Analytical results and (b) corresponding results obtained by the FEM method.

APPENDIX
FIELD EXPRESSIONS

A. TE Modes

$$\mathbf{H}_t = -\frac{j\beta}{k_c^2}\cdot\nabla_t Hz = -\frac{j\beta}{k_c^2}\cdot\left(\frac{\partial}{\partial\rho}Hz\cdot\hat{\rho}+\frac{\partial}{\partial\phi}Hz\cdot\hat{\phi}\right) \tag{31a}$$

Even Modes:

$$= -\frac{j\beta}{k_c^2}\cdot\left(S_{e_n}(h_c,\phi)J'_{e_n}(h_c,\rho)\cdot\hat{\rho} + S'_{e_n}(h_c,\phi)J_{e_n}(h_c,\rho)\cdot\hat{\phi}\right) \tag{31a-i}$$

Odd Modes:

$$= -\frac{j\beta}{k_c^2}\cdot\left(S_{o_n}(h_c,\phi)R'_{o_n}(h_c,\rho)\cdot\hat{\rho} + S'_{o_n}(h_c,\phi)R_{o_n}(h_c,\rho)\cdot\hat{\phi}\right) \tag{31a-ii}$$

$$\mathbf{E}_t = -Z_{TE}\cdot(\hat{\mathbf{z}}\times\mathbf{H}_t) \tag{31b}$$

Even Modes:

$$+Z_{TE}\cdot\frac{j\beta}{k_c^2}\cdot(S_{e_n}(h_c,\phi)J'_{e_n}(h_c,\rho)\cdot\hat{\phi} - S'_{e_n}(h_c,\phi)J_{e_n}(h_c,\rho)\cdot\hat{\rho}) \quad (31b\text{-}i)$$

Odd Modes:

$$= Z_{TE}\cdot\frac{j\beta}{k_c^2}\cdot(S_{o_n}(h_c,\phi)R'_{o_n}(h_c,\rho)\cdot\hat{\phi} - S'_{o_n}(h_c,\phi)R_{o_n}(h_c,\rho)\cdot\hat{\rho}) \quad (31b\text{-}ii)$$

$$Z_{TE}=\eta\cdot\left[1-\left(\frac{f_c}{f}\right)^2\right]^{-1/2} \quad (31c)$$

B. TM Modes

$$\mathbf{E}=-\frac{j\beta}{k_c^2}\cdot\nabla_t Ez=-\frac{j\beta}{k_c^2}\cdot\left(\frac{\partial}{\partial\rho}Ez\cdot\hat{\rho}+\frac{\partial}{\partial\phi}Ez\cdot\hat{\phi}\right) \quad (32a)$$

Even Modes:

$$=-\frac{j\beta}{k_c^2}\cdot(S_{e_n}(h_c,\phi)R'_{e_n}(h_c,\rho)\cdot\hat{\rho} + S'_{e_n}(h_c,\phi)R_{e_n}(h_c,\rho)\cdot\hat{\phi}) \quad (32a\text{-}i)$$

Odd Modes:

$$=-\frac{j\beta}{k_c^2}\cdot(S_{o_n}(h_c,\phi)J'_{o_n}(h_c,\rho)\cdot\hat{\rho} + S'_{o_n}(h_c,\phi)J_{o_n}(h_c,\rho)\cdot\hat{\phi}) \quad (32a\text{-}ii)$$

$$\mathbf{H}_t=\frac{1}{Z_{TM}}\cdot(\hat{\mathbf{z}}\times\mathbf{E}_t) \quad (32b)$$

Even Modes:

$$=-\frac{1}{Z_{TM}}\cdot\frac{j\beta}{k_c^2}\cdot(S_{e_n}(h_c,\phi)R'_{e_n}(h_c,\rho)\cdot\hat{\phi} - S'_{e_n}(h_c,\phi)R_{e_n}(h_c,\rho)\cdot\hat{\rho}) \quad (32b-i)$$

Odd Modes:

$$=-\frac{1}{Z_{TM}}\cdot\frac{j\beta}{k_c^2}\cdot(S_{o_n}(h_c,\phi)J'_{o_n}(h_c,\rho)\cdot\hat{\phi} - S'_{o_n}(h_c,\phi)J_{o_n}(h_c,\rho)\cdot\hat{\rho}) \quad (32b\text{-}ii)$$

$$Z_{TM}=\eta\cdot\left[1-\left(\frac{f_c}{f}\right)^2\right]^{1/2}. \quad (32c)$$

REFERENCES

[1] P. Wilson, D. Hansen, and D. Koenigstein, "Simulating open area test site emission measurement based on data obtained in a novel broadband TEM cell," in *IEEE Nat. Symp. EMC*, Denver, CO, May 23–25, 1989.

[2] S. Ramo, J. R. Whinnery, and T. van Duzer, *Fields and Waves in Communication Electronics*, 2nd Ed. New York: Wiley, 1994, ch. 7, pp. 326–345.

[3] R. E. Collin, *Foundation for Microwave Engineering.* 2nd Ed. New York: McGraw-Hill, 1992, app. III.

[4] P. H. Morse and H. Feshbach, *Methods of Theoretical Physics*, vol. I and II. New York: McGraw-Hill, 1953.

[5] M. Abramowitz and I. A. Stegun, *Handbook of Mathematical Functions.* New York: Dover, 1968.

[6] S. R. Rengarajan and J. E. Lewis, "Mathieu functions of integral orders and real arguments–computer programs description," *IEEE Trans. Microwave Theory Tech.*, vol. MTT-28, pp. 276–287, Mar. 1980.

[7] El-Sherbiny, "Cutoff wavelengths of ridged, circular and elliptic guides," *IEEE Trans. Microwave Theory Tech.*, vol. MTT-21, pp. 7–12, Jan. 1973.

[8] M. N. O. Sadiku, *Numerical Techniques in Electromagnetics.* New York: CRC, 1992.

[9] J. G. Kretzschmar, "Wave propagation in hollow conducting elliptical waveguides," *IEEE Trans. Microwave Theory Tech.*, vol. MTT-18, pp. 547–554, Sept. 1970.

Tullio Rozzi (M'66–SM'74–F'90) received the "Dottore" degree in physics from the University of Pisa, Italy, in 1965, the Ph.D. degree in electronic engineering from Leeds University, Leeds, U.K., in 1968, and the D.Sc. degree from the University of Bath, Bath, U.K., in 1987.

From 1968 to 1978, he was a Research Scientist at the Philips Research Laboratories, Eindhoven, the Netherlands. He spent 1975 at the Antenna Laboratory, University of Illinois, Urbana. In 1978, he was appointed to the Chair of Electrical Engineering at the University of Liverpool, Liverpool, U.K. and was subsequently appointed to the Chair of Electronics and Head of the Electronics Group at the University of Bath, in 1981. From 1983 to 1986, he held the additional position of Head of the School of Electrical Engineering at the University of Bath. Since 1988, he has been Professor of Antennas in the Department of Electronics and Control, University of Ancona, Ancona, Italy, and the Head of the department since 1995, while remaining a visiting professor at Bath University.

Dr. Rozzi is a Fellow of the Institution of Electrical Engineers (IEE), U.K. In 1975 he was awarded the Microwave Prize by the IEEE Microwave Theory and Techniques Society.

Luca Pierantoni (M'94) received the "laurea" degree (summa cum laude) in electronic engineering from the University of Ancona, Ancona, Italy, in 1988, and the Ph.D. degree in electromagnetic fields from the Department of Electronics and Automatics at the University of Ancona, in 1993.

From 1989 to 1996, he was a Research Fellow with the University of Ancona, Department of Electronics and Automatics. His areas of interest are antennas, microwaves, and electromagnetic compatibility. Since 1997, he has been with the Institut für Hochfrequenztechnik Technical University, Munich, Germany.

Marco Ronzitti received the "laurea" degree in electronic engineering from the University of Ancona, Department of Electronics and Automatics, Ancona, Italy, in 1996.

He is currently a Research Fellow with the Department of Electronics and Automatics, University of Ancona,. His areas of interest are antennas, microwaves, and analytical methods for passive devices studies.